Published in final edited form as:
Cell. 2011 June 10; 145(6): 926–940. doi:10.1016/j.cell.2011.04.029.

Paracrine and autocrine signals induce and maintain mesenchymal and stem cell states in the breast

Christina Scheel[1], **Elinor Ng Eaton**[1], **Sophia Hsin-Jung Li**[1,2], **Christine L. Chaffer**[1], **Ferenc Reinhardt**[1], **Kong-Jie Kah**[1,2], **George Bell**[1], **Wenjun Guo**[1], **Jeffrey Rubin**[5], **Andrea L. Richardson**[3], and **Robert A. Weinberg**[1,2,4]

[1] Whitehead Institute for Biomedical Research, Cambridge, MA 02142, USA

[2] Department of Biology, Massachusetts Institute of Technology, Cambridge, MA 02139, USA

[3] Department of Pathology, Brigham and Women's Hospital, Boston, MA 02115, USA

[4] MIT Ludwig Center for Molecular Oncology, Cambridge, MA 02139, USA

[5] National Cancer Institute, 37 Convent Drive, Bethesda, MD 20892-4256

Summary

The epithelial-mesenchymal transition (EMT) has been associated with the acquisition of motility, invasiveness and self-renewal traits. During both normal development and tumor pathogenesis this change in cell phenotype is induced by contextual signals that epithelial cells receive from their microenvironment. The signals that are responsible for inducing an EMT and maintaining the resulting cellular state have been unclear. We describe three signaling pathways, involving Transforming Growth Factor (TGF)-β as well as canonical and non-canonical Wnt signaling, that collaborate to induce activation of the EMT program and thereafter function in an autocrine fashion to maintain the resulting mesenchymal state. Downregulation of endogenously synthesized inhibitors of autocrine signals in epithelial cells enables the induction of the EMT program. Conversely, disruption of autocrine signaling by added inhibitors of these pathways inhibits migration and self-renewal in primary mammary epithelial cells, and inhibits tumorigenicity and metastasis by their transformed derivatives.

Introduction

The epithelial-mesenchymal transition (EMT) effects critical steps of morphogenesis by interconverting epithelial cell types into cells with mesenchymal attributes (Acloque et al., 2009; Thiery et al., 2009). EMT programs activated in carcinoma cells enable them to acquire cellular traits associated with high-grade malignancy, including the ability to complete various steps of the metastatic cascade (Brabletz et al., 2005; Singh and Settleman, 2010). In addition, certain epithelial cells that pass through an EMT acquire the self-renewing trait associated with normal tissue and cancer stem cells (SC/CSC; Mani et al., 2008; Morel et al., 2008). However, the signaling mechanisms that induce and then maintain this mesenchymal/SC state have remained unclear.

Correspondence: weinberg@wi.mit.edu, scheel@wi.mit.edu.

Diverse extracellular signals have been reported to induce EMTs in various cell types (Thiery et al., 2009). In response, pleiotropically acting transcription factors (TFs), such as Twist, Snail, Slug, ZEB1 and ZEB2, are induced that orchestrate EMT programs. We wished to determine whether EMTs induced in human mammary epithelial cells (MEC) by diverse stimuli are manifestations of a common underlying cellular program. In order to characterize mechanisms that induce and subsequently maintain EMT-associated properties in normal and neoplastic MEC, we speculated that autocrine signaling might play a key role in maintaining the mesenchymal/SC state and therefore focused on growth factors and morphogens operating in the extracellular space.

Initially, we utilized a spontaneously arising mesenchymal subpopulation (MSP) of cells isolated from immortalized human MEC (HMLE, Elenbaas et al., 2001). Unlike the parental, largely epithelial HMLE cells, MSP cells resided stably in a mesenchymal/SC state. In this respect, MSP resembled HMLE cells induced to pass through an EMT by overexpression of the Twist EMT-TF (HTwist, Yang et al., 2004). The MSP cells differed significantly from the HTwist cells, since induction and subsequent maintenance of these cells in the mesenchymal/SC state occurred spontaneously and was not provoked by an experimentally predetermined set of signals. Analyses of MSP cells have allowed us to define a set of extracellular signals that operate in a paracrine manner to induce entrance of HMLE cells into the mesenchymal/SC state and subsequently function as autocrine factors to maintain residence in this state. These signals also control the interconversion of primary stem- and progenitor cell-containing, basal MEC, to lineage-restricted, luminal MEC, indicating that they operate in normal mammary gland homeostasis.

Results

A mesenchymal subpopulation (MSP) isolated from immortalized human mammary epithelial (HMLE) cells

We isolated a mesenchymal subpopulation (MSP) of cells that were floating in the medium of monolayer cultures of experimentally immortalized human mammary epithelial (HMLE) cells, similar to the derivation of cell populations described elsewhere (Chaffer et al., in press, PNAS). When transferred to new culture dishes, MSP cells re-attached and could be propagated as adherent cultures (Figures 1A, S1A). In contrast to the epithelial island-forming, parental HMLE cells, the MSP consisted of front-to-back polarized, single cells (Figure 1A,B). Similar to HTwist cells, MSP cells expressed several mesenchymal markers and EMT-TFs (Figure 1B–D, S1B). MSP cells also displayed a $CD44^{hi}/CD24^{-}$ cell-surface marker profile (Figure 1E), suggesting they form part of the naturally occurring $CD44^{hi}/CD24^{-}$ SC subpopulation within HMLE cell cultures (Mani et al., 2008).

The mammosphere assay measures anchorage-independent proliferation at clonal density *in vitro* and has been associated with the presence of mammary epithelial progenitor and SC populations (Dontu et al., 2003). We therefore used the mammosphere-forming abilities of these various cell populations to gauge their content of SCs. Relative to the parental HMLE cells, FACS-isolated $CD44^{hi}/CD24^{-}$ HMLE cells were 5-fold, the MSP cells 12-fold, and the HTwist cells 18-fold enriched in mammosphere-forming cells (Figure 1F).

To test for another functional hallmark of mesenchymal/SC, we conducted *in vitro* motility assays. HTwist cells were most migratory (45-fold compared to bulk HMLE cells), followed by MSP cells (30-fold) and FACS-purified $CD44^{hi}/CD24^{-}$ cells (12-fold, Figure 1G). We noted that the majority epithelial population of parental HMLE cells displayed a $CD44^{-med}/CD24^{+}$ cell-surface marker profile. When isolated by Magnetic Activated Cell Sorting (MACS) or FACS, this population was depleted of mammosphere-forming and migrating cells, suggesting the latter were contained exclusively within the $CD44^{hi}/CD24^{-}$ population

(Figure 1F,G). Together, our observations indicated that spontaneously arising MSP cells represent a $CD44^{hi}/CD24^{-}$ subpopulation enriched for motile, mammosphere-forming cells.

Comparative profiling of the autocrine signaling context

We speculated that maintenance of the mesenchymal/SC state might depend on the activation of autocrine signaling loops, as has been suggested for TGF-β-induced EMT in *RAS*-transformed mouse MEC (Oft et al., 1996). To test this notion, we studied secreted proteins released into the culture medium of MACS-purified $HMLE^{24+}$ and HTwist cells using antibody arrays and extended these findings to the above-described MSP cells (Figure S1C-E, Table S1). Based on functional grouping, secreted factors associated with passage through an EMT contained predominantly pro-angiogenic factors and proteins acting in the Wnt and TGF-β signaling pathways (Table S2). For our initial studies, we focused on factors likely to function in an autocrine rather than paracrine manner on other cells within the tissue microenvironment; accordingly, the work described below emphasizes Wnt and TGF-β signaling.

We complemented the above analyses with microarray gene expression profiling of $HMLE^{24+}$ and three independently derived MSP cell lines. Cluster analysis with a previously published "EMT core signature" based on HMLE cells ectopically expressing various EMT-TFs, including Twist (Taube et al., 2010), revealed significant overlap with the three MSP cell lines, whereas the $HMLE^{24+}$ cells clustered with the bulk HMLE cells (Table S3,S4).

EMT-associated autocrine signaling: activation of TGF–β and restriction of BMP signaling

We initially focused on TGF-β signaling. We noted increased secretion of TGF–β1 protein by HTwist and MSP cells, relative to $HMLE^{24+}$ cells (Figure 2A), correlating with increased activity (1.5-2-fold) of a Smad-reporter plasmid (SBE4-luc, Figure 2B) and Smad2 phosphorylation (Figure 2C), all indicators of active TGF-β signaling. We noted that MSP cells propagated in culture medium depleted of all growth factors retained Smad2 phosphorylation, supporting an autocrine origin of TGF-β (Figure 2D).

Our attention was also drawn to possible modulation of TGF-β by BMP signaling: mutual antagonism of TGF-β and BMP signaling pathways at several levels has been described (Guo and Wang, 2009), and BMP signaling is known to antagonize the TGF-β-driven EMT occurring during renal fibrosis (Zeisberg et al., 2003). In our own hands, secreted protein and gene expression profiling revealed two secreted BMP antagonists, Chordin-like 2 and Gremlin to be significantly upregulated in MSP and HTwist compared to HMLE cells; this was confirmed by RT-PCR (Figure 2E).

These observations led us to interrogate the expression status of BMP ligands by RT-PCR: relative to their mRNA expression in the parental HMLE cells, several BMP ligands were strongly downregulated in both HTwist and MSP cells (Figure S2A). This suggested that TGF-β signaling might be enabled in the HTwist and MSP cells through down-regulation of BMPs and upregulation of two BMP antagonists. Consequently, we tested whether TGF-β signaling could be modulated by the presence of BMP-antagonists. Indeed, we observed an increase of Smad2 nuclear translocation in epithelial $HMLE^{24+}$ cells stimulated with low doses of TGF-β in the presence of recombinant Gremlin or Chordin-like 2, relative to TGF-β introduced on its own. This effect was presumably achieved through neutralization by Gremlin and Chordin-like 2 of endogenously expressed BMP ligands (Figure 2F). Conversely, nuclear translocation of Smad2 following stimulation with a high concentration of TGF-β, presumably high enough to overcome inhibitory signals by endogenous BMP

production, could be inhibited by concomitant addition of recombinant BMP4 to the growth medium (Figure 2F).

Together, these observations indicated that HTwist and MSP cells exhibit an extracellular signaling environment that restricts BMP signaling via (1) loss of BMP ligand production and (2) upregulation of the secreted Chordin-like 2 and Gremlin BMP antagonists. Given the above-mentioned role of BMP as a TGF-β antagonist, this suggested that cells that have passed through an EMT are more responsive to extracellular TGF-β ligand, including the ligand that they secrete. Indeed, when we treated $HMLE^{24+}$ in parallel with MSP cells with recombinant TGF-β, we found that MSP cells were more responsive, as gauged by a 3- to 5-fold greater nuclear translocation of Smad 2/3 as well as SBE4-luc reporter activity (Figure S2B).

EMT-associated autocrine signaling: canonical and non-canonical Wnt signaling

We wished to determine whether Wnt signaling pathways, identified above as being activated upon entrance into a mesenchymal state, collaborated with TGF-β signaling in MSP and HTwist cells. First, we found that secretion of the canonical Wnt signaling antagonist Dickkopf-1 (DKK1, Kuhnert et al., 2004), was downregulated in both HTwist and MSP cells (Figure 2G). Second, gene expression of the Secreted Frizzled Related Protein-1 (SFRP1), which sequesters both canonical and non-canonical Wnt ligands in the extracellular space (Suzuki et al., 2004), was downregulated in HTwist and undetectable in MSP relative to $HMLE^{24+}$ cells (Figure 2H). Of the multiple SFRPs encoded in the genome, SFRP1 was the only one expressed at significant levels in $HMLE^{24+}$ relative to MSP cells (Figure S2C). We also examined whether production of Wnt ligands was changed upon passage through an EMT. RT-PCR analysis revealed up-regulation of non-canonical Wnt ligands 5a and 16 in HTwist and MSP cells (confirmed by immunoblotting for Wnt5a, Figure 2L), whereas other Wnt ligands were expressed at comparable levels (Wnt2, 2b and 6) or downregulated (Figure S2D).

We measured the activity of β-catenin-dependent canonical Wnt signaling pathway using the TOPFlash β-catenin/TCF-LEF reporter assay (Veeman et al., 2003). Doing so revealed a 5-fold higher TOP relative to FOP (control) activity in HTwist, and a 20-fold higher TOP/FOP activity in the MSP cells (Figure 2J). In contrast, β-catenin/TCF-LEF activity was undetectable in the $HMLE^{24+}$ cells. In addition, mRNA levels of Axin2, a conserved β-catenin/TCF-LEF target gene were upregulated 15- and 30-fold in HTwist and MSP cells, relative to $HMLE^{24+}$ cells (Figure 2I). Together, these observations indicated that β-catenin-dependent, canonical Wnt signaling was active in HTwist and MSP cells but not in the parental $HMLE^{24+}$ cells. Because no Wnt ligand was present in the medium, we concluded that canonical Wnt signaling operated in an autocrine manner. Importantly, the observed concomitant downregulation of Wnt antagonists appeared to be a rate-limiting determinant of β-catenin/TCF-LEF transcriptional activity, as suggested previously for certain breast and colon cancer cell lines (Bafico et al., 2004; Suzuki et al., 2004). Thus, we found that addition of either recombinant DKK1 or SFRP1 proteins resulted in 1.5- and 2-fold reduction of TOPFlash reporter activity in the HTwist and MSP cells, respectively (Figure 2K).

We also analyzed the activity of non-canonical Wnt signaling pathways in HTwist and MSP cells; as mentioned above, production of the non-canonical Wnt5a ligand was strongly upregulated in the MSP and HTwist cells (Figure 2L). Wnt5a binding to non-canonical Frizzled receptors has been shown to activate protein kinase C (PKC) isoforms (Dissanayake et al., 2007). Indeed, we observed significant levels of activated PKCs in HTwist and MSP cells, but not in the $HMLE^{24+}$ cells (Figure 2L). In addition, JNK signaling has been shown to be activated by Wnt5a and to mediate breast cancer invasion

(Pukrop et al., 2006). We found elevated phosphorylation of JNK and its downstream target, c-Jun, in HTwist and MSP relative to the parental HMLE^{24+} cells (Figure 2L). These results suggested that autocrine non-canonical Wnt signaling was active in HTwist and MSP cells, acting via at least two downstream pathways involving the PKC and JNK proteins.

Autocrine Signaling controls migration and mammosphere formation

The above experiments indicated that autocrine canonical and non-canonical Wnt as well as TGF-β signaling pathways were active in MSP and HTwist cells. To address whether ongoing autocrine signaling was instrumental in maintaining residence in the mesenchymal/SC state, we added back to cultured HTwist and MSP cell cultures some of the secreted inhibitory factors that we found to be downregulated relative to the parental HMLE^{24+} cells, and assessed effects on motility and mammosphere-forming ability.

Addition of either recombinant DKK1 or SFRP1 to the culture medium of HTwist and MSP cells inhibited migration in a dose-dependent manner (Figure 3A and B). At the highest concentration, recombinant DKK1 reduced migration 10-fold, SFRP1 20-fold (Figure 3A and B). BMP4 had a less potent effect on migration, inducing a 2-fold reduction in HTwist and MSP cells (Figure 3C). Of note, proliferation of adherent HTwist and MSP cultures was not affected by these proteins, excluding general cytostatic and cytotoxic effects (Figure S3A).

To test the effects of Wnt antagonists and BMP ligands on mammosphere-forming ability, we added various proteins daily for a period of 5d beginning from initial seeding of cells. We then dissociated the initially formed mammospheres, and re-introduced these cells into secondary mammosphere cultures in the absence of further treatment. We observed a modest reduction of sphere formation by DKK1 (Figure 3D,E). SFRP1 and BMP4 had a more potent effect, reducing secondary sphere formation by 80–90% in MSP and HTwist cells (Figure 3E). Taken together, these data indicated that SFRP1 and BMP4, and to a lesser extent DKK1, inhibit migration as well as self-renewal.

We also tested cooperative effects of these factors. Thus, we added either DKK1 or SFRP1 in combination with BMP4 to HTwist cells: doing so inhibited migration in an additive manner (8- and 7-fold respectively, compared to 3-, 5- and 2-fold when added individually, Figure 3F). During primary mammosphere formation, we observed a 74% reduction in sphere-forming efficiency when DKK1 or SFRP1 were added together with BMP4 (Figure 3G). This compared to 40% reduction when either DKK1 or SFRP1 was added singly, and a 64% reduction when BMP4 was added singly.

These responses suggested that the three classes of secreted signaling proteins work, at least in part, through distinct downstream pathways. To inhibit autocrine TGF-β signaling directly, we used pharmacologic inhibitors of the TGF-β Receptor Type I (TGFBRI); these attenuated migration and mammosphere formation of HTwist and MSP cells to a similar extent as added BMP4 protein (Figure S3D–E). However, the combination of a TGFBRI inhibitor and BMP4 did not have an additive effect (Figure S3D), suggesting that BMP4 exerts most of its inhibitory effects by interfering with TGF-β signaling.

Our findings emphasize the importance of ongoing autocrine signaling in maintaining the mesenchymal/SC state of the MSP cells. More surprising were the observed effects on HTwist cells (Figure 3A–E), suggesting that continuous expression of the EMT-inducing Twist TF cannot maintain residence in the mesenchymal/SC state through intracellular signaling, but instead depends on extracellular autocrine signaling loops. To further test this notion, we induced an EMT in HMLE cells using a conditional Twist-ER expression vector (Casas et al., 2011). We induced Twist expression for 12d by application of tamoxifen, after

which these HTwist-ER cells maintained a stable, mesenchymal/SC state in the absence of further tamoxifen, presumably due to induced expression of endogenous EMT-TFs (Figure S3F). Indeed, these cells remained sensitive to inhibition of migration and mammosphere formation by SFRP1, BMP4 and a TGFBRI inhibitor (Figure S3G,H).

Autocrine signaling controls tumorigenicity and metastasis of MSP-RAS cells

We also wished to determine whether autocrine loops maintain the tumorigenic and metastatic behaviors of the *RAS* oncogene-transformed derivatives of HMLE cells. To begin, we measured the tumor-initiating frequency of *RAS*-transformed MSP and HMLE^{24+}-cell populations. Similar to previously published results (Mani et al., 2008), implantation of 1×10^5 HMLE^{24+}-RAS cells was necessary for subcutaneous tumor formation, whereas HTwist-RAS and MSP-RAS populations were enriched for tumor-initiating cells by at least two orders of magnitude (Figure S4A,B). Moreover, two independently isolated MSP-RAS populations exhibited a 10-fold increased ability to seed metastatic foci in the lung compared to HMLE^{24+}-RAS cells (Figure S4C-G).

Exposure *in vitro* of MSP-RAS cells to SFRP1 protein reduced motility 9-fold, to BMP4 4-fold, and to a combination treatment 30-fold (Figure 4A). Importantly, proliferation of MSP-RAS cells in monolayer culture was unaffected by the presence of these recombinant proteins (Figure S4H).

As a surrogate assay for tumor-initiating ability, we tested the formation of tumorspheres in 3-dimensional cultures at clonal densities (Fillmore and Kuperwasser, 2008). MSP-RAS cells treated with recombinant SFRP1 and BMP4 during primary tumorsphere formation displayed a reduction in both primary as well as secondary sphere formation by 40% when each factor was added alone, and by 60% when added in combination (Figure 4B). Together, these data indicated that autocrine signaling continues to control migratory and self-renewal ability in MSP cells following transformation by a *RAS* oncogene.

To determine whether *in vitro* exposure to SFRP1 and BMP4 influenced subsequent *in vivo* behavior of MSP-RAS cells, we prepared single-cell suspensions from MSP-RAS tumorspheres and implanted them orthotopically in mice. We noted that tumors originating from mammospheres of MSP-RAS cells exposed *ex vivo* to either SFRP1, BMP4 or a combination of both were reduced in weight by 3-fold on average (Figure 4C, S4J). We observed a modest reduction in tumor incidence for the BMP4- and combination-treated groups (30%), suggesting that sufficient numbers of tumor-initiating cells remained which were, however, compromised in their ability to vigorously proliferate and/or survive *in vivo*.

Further, we noted a 2-fold reduction in lung metastases in the SFRP1-treated group, 7.5-fold in the BMP4-, and 4.5-fold in the combination-treated group (Figure 4E). Echoing the effects on migration *in vitro*, combination treatment with SFRP1 and BMP4 had a synergistic effect in decreasing the number of metastatic foci in the liver, by >10-fold on average, compared to a 2.5- and 5-fold reduction in the mice bearing cells treated *ex vivo* with SFRP1 or BMP4 singly (Figure 4F,G).

We speculated that exposure to SFRP1 and BMP4 following implantation in mouse hosts might exert a stronger effect on the tumor-initiating ability of MSP-RAS cells. Accordingly, we implanted these cells subcutaneously in limiting dilutions in Matrigel plugs impregnated with SFRP1, BMP4, or a combination of both (Figure 4G). In addition, recombinant proteins at indicated doses were injected peritumorally 1, 2, 3 and 7 days after implanting the MSP-RAS cells. We found that exposure to SFRP1, BMP4 or combination treatment reduced tumor incidence by at least one order of magnitude (Figure 4H). Together, these

observations demonstrated that similar regulatory loops were operative in the immortalized HMLE cells and their transformed derivatives.

Creation of a permissive extracellular environment promotes the induction of an EMT in HMLE cells

The above experiments revealed that ongoing autocrine signaling through Wnt and TGF-β pathways was important for maintaining the migratory and self-renewal abilities of cells that resided in the mesenchymal/SC state. It remained possible that these same pathways could activate an EMT program in epithelial cells. To examine this, we treated $HMLE^{24+}$ cells with TGF-β, the first extracellular factor reported to induce an EMT (Oft et al., 1996). However, treatment of $HMLE^{24+}$ cells for a period of 3d with TGF-β, titrated to elicit maximal Smad2-phosphorylation (Figure S5A), did not result in a change in expression of mRNAs encoding epithelial and mesenchymal markers, and EMT-TFs (Figure 5A). These data echoed previous observations demonstrating that TGF-β on its own rarely induces an EMT (Brown et al., 2004).

We therefore explored contributions of additional signaling pathways to activation of the EMT program in $HMLE^{24+}$ cells. These involved: (1) Modulation of Wnt signaling: to reduce Wnt inhibition, we added a DKK1-neutralizing antibody and knocked down expression of the SFRP1-encoding mRNA (Figure S5B). We also added recombinant Wnt5a, since Wnt5a was upregulated in HTwist and MSP cells. (2) Destabilization of adherens junctions: we added an anti-E-cadherin antibody; previous work suggested that loss of E-cadherin is a rate-limiting step for EMT (Onder et al., 2008).

To summarize our findings, only the presence of all of these EMT-inducing components plus recombinant TGF-β1, which together constituted the EMT induction cocktail (IC), led to a significant induction of the mesenchymal marker N-cadherin and the ZEB1 and ZEB2 EMT-TFs in $HMLE^{24+}$ cells (Figure 5A, S5C,D).

Creation of a permissive extracellular environment for stable expression of mesenchymal/SC traits

To investigate whether the initiation of an EMT triggered by the IC would yield cells that entered stably into the mesenchymal/SC state, we treated $HMLE^{24+}$ cells with TGF-β alone or with the above-described IC, Figure 5A). Over 14d, IC-treated cells acquired a mesenchymal morphology while control and TGF-β treated cells remained epithelial (Figure S5E,F). During 12 subsequent passages (~36 population doublings) following cessation of treatment, IC-treated cells remained mesenchymal and did not revert back to an epithelial morphology.

In such phenotypically stable IC-treated cells, but not in those treated only with TGF-β, we observed a switch from E- to N-cadherin expression and an upregulation of the Vimentin and Fibronectin mesenchymal markers (Figure 5B, S5G,I). RT-PCR analysis of ZEB1, ZEB2 and Twist EMT-TFs provided further evidence that IC-treated cells had moved stably into a mesenchymal state: these mRNAs were upregulated >100-fold compared to control cells and those treated with TGF-β alone (Figure S5G).

On the basis of the work presented above, we speculated that autocrine signaling loops involving the same factors that had previously triggered entrance into an EMT were established in these IC-treated cells. Indeed, relative to control and TGF-β-treated cells, we observed a 3- to 4-fold increase in Smad-reporter activity (Figure S5H) and Smad2 phosphorylation (Figure S5I). In IC-treated cells, we detected cytoplasmic and nuclear β-catenin (Figure 5B) as well as β-catenin/TCF-LEF reporter activity, indicative of canonical

Wnt signaling (Figure S5H). We also measured increased levels of Wnt5a and elevated phosphorylation of PKCs and JNK, indicative of non-canonical Wnt signaling (Figure S5I).

Relative to control cells, IC-treated cells formed 70 times more mammospheres, and their ability to migrate increased 50-fold (Figure 5C,D). In contrast, cells treated only with TGF-β displayed a small increase in mammosphere-forming efficiency (10-fold) but not in motility. Echoing these results, we observed a comparably small increase in the proportion of $CD44^{hi}/CD24^{-}$ cells in TGF-β-treated cells (from 0.2% to 1.5%) compared to the 98% representation of $CD44^{hi}/CD24^{-}$ cells in IC-treated cultures (Figure 5F).

Importantly, these effects could not be attributed to increased proliferation of the IC-, and TGF-β-treated cells; their proliferation rates were lower than those of control cells (Figure S5F). Moreover IC-treated cells remained sensitive to perturbation of their autocrine environment: treatment of these cells with SFRP1, BMP4 or a combination of both inhibited migration and mammosphere formation (Figure 5E,F). Finally, when these various cell populations were transformed with a *RAS* oncogene, IC-treated cells, implanted into the mammary fat pads of mice, gave rise to lung metastatic foci with a similar elevated frequency as MSP-RAS cells. By contrast, control and TGF-β-treated cells were only weakly metastatic (Figure 5G,H).

Together, these various findings indicated that the same factors involved in maintaining the mesenchymal/SC state can also serve to induce entrance into this state, allowing the derivation of cells with stable migratory and SC properties from populations that previously displayed these functional attributes at very low levels.

Characterization of primary mammary epithelial cell populations enriched in self-renewal and motility

We set out to explore whether the autocrine loops that govern migratory and self-renewal traits in HMLE cells and their transformed derivatives were also operative in cell populations residing within the human mammary gland. In fact, stem and progenitor cells had been previously resolved within $CD49f^{+}/EpCAM^{-}$ MEC populations (Eirew et al., 2008). Accordingly, we prepared $CD49f^{+}$ MEC populations from reduction mammoplasties that were either positive or negative for expression of EpCAM by FACS (MEC^{EPC+} or MEC^{EPC-}, Figure S6A) and conducted mammosphere assays to test for the presence of stem and progenitor cells. We found that unsorted MEC displayed a mammosphere-forming frequency of 0.15–0.5%, comparable to previous reports (Dontu et al., 2003). In contrast, 1–2% of MEC^{EPC-} cells formed mammospheres, relative to 0.1–0.3% of MEC^{EPC+} cells (Figure 6A).

We noted that MEC^{EPC+} formed epithelial islands, whereas MEC^{EPC-} displayed a scattered mesenchymal morphology (Figure S6B). Both MEC^{EPC-} and MEC^{EPC+} cells expressed cytokeratins at similar levels; however, the MEC^{EPC-} cells additionally expressed high levels of the mesenchymal marker vimentin (Figure 6C). Despite similar levels of E-cadherin mRNA (Figure S6C), MEC^{EPC-} did not form adherens or tight junctions (Figure 6C). We next assessed the expression of EMT-TFs and observed high expression levels of Slug, Twist, ZEB1 and ZEB2 in MEC^{EPC-}, but not MEC^{EPC+} cells (Figure 6D, S6D). These data indicated that mesenchymal properties were displayed specifically by populations of cells enriched for self-renewal, similar to the phenotypes of the MSP and HTwist cells studied previously.

In light of their mesenchymal morphology, we assessed whether MEC^{EPC-} displayed increased motility. Indeed, MEC^{EPC-} had a 20-fold greater ability to migrate *in vitro* relative to unsorted bulk MEC and 40-fold relative to MEC^{EPC+} cells (Figure 6B). Further, we found

a 2-fold enrichment in mammosphere formation in migrated MEC^{EPC-} collected from the bottom of migration chambers compared to monolayer-grown MEC^{EPC-}, suggesting a link between motility and mammosphere-forming ability (Figure S6E).

To align these primary MEC populations with known mammary gland lineages, we assessed the expression of lineage markers in MEC^{EPC+} cells and in MEC^{EPC-}. These analyses showed enrichment in the expression of basal markers in MEC^{EPC-} (p63, cytokeratin 14, α-smooth muscle actin) and of luminal markers in MEC^{EPC+} (Mucin-1, cytokeratin 8, 18, Figure S6F). We concluded that MEC^{EPC-} cells represented populations of the basal lineage showing a mesenchymal, migratory and mammosphere-enriched phenotype, whereas the MEC^{EPC+} cells exhibited epithelial traits and luminal differentiation.

Wnt and TGF-β signals govern interconversions between basal and luminal MEC

We investigated whether the autocrine loops operative in HTwist and MSP cells were also active in MEC^{EPC-} populations. Indeed, we observed high mRNA levels of Axin2 (Figure S6G) as well as cells with cytoplasmic/nuclear β-catenin and nuclear Smad2 in the MEC^{EPC-} but not in the MEC^{EPC+} (Figure 6E, S6H).

We then tested the effects of inhibiting autocrine signaling on mammosphere formation and motility. Because recombinant BMP4 exerted a strong anti-proliferative effect on primary MEC (data not shown), we inhibited TGF-β signaling in parallel with two different TGFBRI-kinase inhibitors and blocked autocrine Wnt signaling through application of recombinant SFRP1. A 5d pre-treatment of MEC^{EPC-} cells with the TGFBRI inhibitors or with SFRP-1 reduced subsequent mammosphere formation by 80–90% (Figure 6F). Furthermore, we observed a complete inhibition of motility by pre-treatment with the TGFBRI inhibitors, and a 3-fold reduction by SFRP1 (Figure 6G). Importantly, inhibition of these autocrine loops did not reduce the proliferation of MEC^{EPC-} in monolayer cultures (Figure S6I).

When added at lower concentrations, TGFBRI inhibitors added together with SFRP1 had a synergistic effect in suppressing mammosphere formation (84% reduction jointly compared to ~50% when each was added alone, Figure S7A). We also found that a 5 day-long treatment with either TGFBRI inhibitor or SFRP1 yielded increased tight and adherens junction formation in MEC^{EPC-} (Figure S7C) and reduced the expression of Slug and p63, as gauged by immunofluorescence and RT-PCR (Figure S7B,C). Indeed, following combination treatment of TGFBRI inhibitor together with SFPR1, transcript levels of p63 and Slug were reduced to levels comparable to those in MEC^{EPC+}, whereas Claudin-2 mRNA, associated with the epithelial state, was upregulated (Figure S7B), suggesting a luminal differentiation process.

Analogous to our earlier experiments, we also determined whether the EMT-IC could be applied to MEC^{EPC+} to induce migratory and mammosphere-forming abilities. We found that a 5d pre-treatment of MEC^{EPC+} with either TGF-β, E-cadherin antibody, or a combination of neutralizing DKK1 and SFRP1 antibodies together with Wnt5a (functioning as activators of the canonical and non-canonical Wnt pathways respectively) increased subsequent migration and mammosphere formation 3-5-fold. However, when added together, these factors did not function in either an additive or synergistic manner (Figure S7D,E).

We speculated that a sequential activation of Wnt and TGF-β signaling might allow MEC^{EPC+} to respond to both signals. Indeed, a 3d pre-treatment with the Wnt activators prior to addition of TGF-β, E-cadherin antibody, or a combination of both for an additional 2d resulted in a synergistic increase of migration and mammosphere formation (Figure

7A,B). Importantly, when primary mammospheres were dissociated and placed into secondary sphere assays, we observed an expansion of the proportion of sphere-forming cells only in MEC^{EPC+} that had been treated with all factors, reaching a representation similar to that observed in MEC^{EPC-} (Figure 7B).

Additionally, MEC^{EPC+} cells exposed to all agents present in the IC showed the greatest decrease in junctional E-cadherin, β–catenin and ZO-1 expression and greatest increase in Slug and p63 expression (Figure 7C,D). By contrast, various combinations of these factors led to partial EMT phenotypes with mild disruption of adherens and tight junction formation. Importantly, the highest levels of nuclear Smad2 as well as cytoplasmic and nuclear beta-catenin and upregulation of Axin2 mRNA were observed in MEC^{EPC+} cells exposed to the IC, indicating establishment of autocrine Wnt and TGF–β signaling (Figure 7C,D). Together, these data demonstrated a remarkable plasticity in MEC^{EPC+}: exposure of these cells to DKK1-, SFRP1- and E-cadherin-neutralizing antibodies, together with TGF-β and Wnt5a resulted in the collaborative induction of mesenchymal and basal traits, as well as motility and mammosphere-forming ability.

Discussion

An array of contextual signals has been implicated in the induction of an EMT, almost invariably in cells that have undergone unknown predisposing genetic changes (Thiery et al., 2009). Using both primary normal, immortalized, and neoplastic human MEC, we demonstrate that the EMT program cannot be efficiently induced by activation of one or another signaling pathway. Instead, multiple pathways must collaborate with one another to do so.

The present data extend an experimental paradigm described 14 years ago, when it was shown that TGF-β is able to induce an EMT in *RAS*-transformed mouse MEC (Oft et al., 1996). In our hands, TGF-β signaling, while necessary, is not sufficient for this conversion in human MEC and instead requires collaboration of two Wnt signaling pathways. Our observations indicate that some of the factors necessary for the induction of these three EMT-inducing autocrine signaling loops are secreted by cells that reside in an epithelial state. However, these factors fail to establish autocrine signaling loops because of the concomitant secretion of inhibitors. Accordingly, a permissive environment for the induction of an EMT can be created by reducing the levels of secreted inhibitors of these pathways, specifically SFRP1, DKK1, and BMPs. Future studies are needed to determine directly whether such a mechanism operates in the intact mammary gland and, more generally, in the homeostasis of other epithelial tissues. Thus, it remains to be demonstrated that the signaling circuits critical to EMT induction in human MEC operate as well in a variety of others epithelial cell types.

Once cells have passed through an EMT, both normal and neoplastic MEC maintain their residence in the resulting mesenchymal/SC state by ongoing autocrine signaling, doing so through the same signals that previously induced entrance into this state. Thus, we observed that after a 14-day treatment period, continued exposure to the EMT-induction cocktail (IC) was no longer required. Our data suggest this is due to the establishment of a network of mutually reinforcing autocrine loops engaging both Wnt and TGF-β pathways. These autocrine loops presumably serve to ensure continued expression of the EMT transcriptional circuitry. Indeed, during experimental induction of an EMT, we observed activation of the expression of several EMT-inducing TFs, notably Slug, Twist, ZEB1 and ZEB2. Further support of this biological concept comes from the work of others, demonstrating that embryonic (Ogawa et al., 2007), muscle (Abou-Khalil et al., 2009), mesenchymal (Rider et

al., 2008) and neural SC (Toda et al., 2003) secrete growth factors in an autocrine manner to protect themselves from spontaneous differentiation and to support their self-renewal.

Responding to these findings, we suggest that residence in the mesenchymal/SC state can be destabilized if extracellular autocrine loops are disrupted by exposure to their endogenous inhibitors, i.e., the Wnt antagonists DKK1 and SFRP1 as well as BMPs. Thus, in our own hands, disruption of autocrine signaling leads to the reduction of migratory and mammosphere-forming ability in immortalized MEC, and to inhibition of metastasis and tumor-initiating ability in their transformed derivatives.

We find that the same set of signals that induce and maintain mesenchymal/SC traits via induction of an EMT program in immortalized and transformed HMLE cells, also governs interconversions between primary SC/progenitor cell-enriched (basal) and lineage-restricted (luminal) MEC. These data suggest that, given a permissive signaling context, a high degree of plasticity exists within normal MEC populations and provide direct support for the emerging notion that normal and neoplastic epithelial cells utilize very similar SC programs.

A number of additional factors have been found capable of inducing an EMT in a variety of epithelial cell types, including Notch, Sonic Hedgehog and various growth factors that activate tyrosine kinase receptors. We suggest that the physiologic relevance of these factors and their roles in maintaining the mesenchymal/SC state can be gauged by studying epithelial cells of various tissue origins that undergo spontaneous entrance into this state, such as the MSP cells we describe in this manuscript. Such work may reveal alternative mechanisms of stabilizing residence in the mesenchymal/SC state in other epithelial tissues. It also remains possible that the pathways described here represent core EMT-inducing signals shared in common by a variety of epithelial cell types, and that other documented EMT-inducing signaling pathways ultimately converge on the three studied here.

In the longer term, the present observations may provide the basis for efficiently inducing differentiated epithelial cells to pass through an EMT and enter into a SC state without relying on genetic alteration, such as introduction of genes specifying EMT-TFs. Such an approach may eventually be of great utility in the area of regenerative medicine in those instances where the rapid regeneration of damaged epithelial tissues is required. Acting in the opposing direction, the tumor-initiating cells of certain carcinomas may be forced to exit the mesenchymal/SC state by therapeutically interrupting multiple autocrine signaling pathways required for their continued residence in this state.

Experimental Procedures

Antibody arrays and Microarrays

Supplemental Experimental Procedures.

Cell lines

Supplemental Experimental Procedures.

Primary mammary epithelial cell culture

Supplemental Experimental Procedures.

Plasmids, virus preparation, transfection and infection of cells

Supplemental Experimental Procedures.

Migration and invasion assays

25,000 cells were seeded into 24-well cell culture inserts with 8-μm pores (BD Falcon). After 12–48h, the cells on the upper surface of the filters were removed with a cotton swab. For visualization, cells on lower filter surfaces were fixed and stained with a Diff-Quick staining kit (Dade Behring). 3–5 fields/filter were counted. Data are presented as migrated cells/field.

Mammosphere and tumorsphere assay

Assays were performed as previously described with modifications (Dontu et al., 2003): 1000 cells/well were seeded in 96-well ultra-low adhesion plates (Corning) in MEGM medium containing 1.3% methylcellulose (Stem Cell Technologies) supplemented with 20ng/ml EGF, 10ng/ml bFGF (Sigma) and B27 (Gibco). For secondary sphere formation, primary spheres were dissociated by trypsinization and replated at 1000 cells/well.

Animal studies

Research involving animals complied with protocols approved by the MIT Committee on Animal Care. For tumorigenicity studies, cells suspended in 100 μl of a Matrigel/PBS mix (BD Biosciences) were injected subcutaneously in the flanks of age-matched nude (nu/nu) mice. Mice were sacrificed and necropsied after 10 weeks. For orthotopic injections, 1×10^5 cells suspended in PBS were injected into the inguinal mammary glands of age-matched female NOD/SCID mice. Mice were sacrificed after 10 weeks or when tumors reached a diameter >1cm. For tail vein injections, 1×10^5 cells suspended in PBS were injected into the tail vein of age-matched, male NOD/SCID mice. Lung surface metastases were counted using a fluorescent microscope.

Recombinant proteins and inhibitors

Supplemental Experimental Procedures.

Antibodies

Supplemental Experimental Procedures.

Immunoblots

Protein was extracted with RIPA lysis buffer. Protein lysates were resolved on a 4%–12% Bis-Tris Gel, transferred to PVDF membranes, probed with HRP-linked secondary antibodies (GE Healthcare) and visualized with ECL reagent (Thermo Scientific).

Immunofluorescence

Cells were grown on Labtek II-CC2 Chamber slides (Nunc), fixed with 4% paraformaldehyde and permeabilized with 0.2% Triton-X-100/PBS prior blocking with 10% goat serum (Caltag). Secondary antibodies were goat-anti-mouse or –rabbit coupled to Alexa-488 or −594 (Invitrogen). Cell nuclei were visualized with DAPI (Sigma). Slides were mounted with SlowFade Gold antifade reagent (Invitrogen).

Fluorescent activated cell sorting (FACS) and flow cytometry

Cells were prepared according to standard protocols and suspended in 0.1%BSA/PBS on ice prior FACS. 7-AAD (BD Biosciences) was used to exclude dead cells. Cells were sorted on a BD FACSAria SORP and analyzed on a BD LSRII using BD FACSDiva Software (BD Biosciences).

RNA preparation and RT-PCR analysis

RNA was isolated with the RNeasy Micro kit (Qiagen). Reverse transcription was performed with the Superscript III First Strand Synthesis kit (Invitrogen). SYBR Green Mix I (Roche Diagnostics) was used for amplification and samples were run on a Lightcycler-II Instrument (Roche Diagnostics). Analysis was described previously (Yang et al., 2004). L32 was used as loading control, n=3. Primers are listed in Table S5.

Statistical analysis

Data are presented as mean+/−SEM. Student's t test (two-tailed) was used to compare two groups ($p<0.05$ was considered significant) unless otherwise indicated.

Supplementary Material

Refer to Web version on PubMed Central for supplementary material.

Acknowledgments

We thank Brian Bierie, Thijn Brummelkamp, Sunny Gupta, Katharina Leuchte, Julia Rastelli, Andreas Scheel, Scott Valastyan and Irene Wuethrich for critical reading of the manuscript; members of the Weinberg lab for discussion; John Stingl for protocols; the Whitehead Microarray and Flow Cytometry Cores, and the W.M. Keck Microscopy Facility for technical support. This research was supported by the NIH/NCI (R.A.W.: CA12515 and DE020817), MIT Ludwig Center for Molecular Oncology (R.A.W.), Ludwig Fellowship for Metastasis Research (C.S.), Breast Cancer Research Foundation (A.L.R., R.A.W.), Harvard Breast Cancer SPORE (A.L.R., R.A.W.) and DoD BCRP Idea Award (R.A.W.).

References

Abou-Khalil R, Le Grand F, Pallafacchina G, Valable S, Authier FJ, Rudnicki MA, Gherardi RK, Germain S, Chretien F, Sotiropoulos A, et al. Autocrine and paracrine angiopoietin 1/Tie-2 signaling promotes muscle satellite cell self-renewal. Cell Stem Cell. 2009; 5:298–309. [PubMed: 19733541]

Acloque H, Adams MS, Fishwick K, Bronner-Fraser M, Nieto MA. Epithelial-mesenchymal transitions: the importance of changing cell state in development and disease. J Clin Invest. 2009; 119:1438–1449. [PubMed: 19487820]

Bafico A, Liu G, Goldin L, Harris V, Aaronson SA. An autocrine mechanism for constitutive Wnt pathway activation in human cancer cells. Cancer Cell. 2004; 6:497–506. [PubMed: 15542433]

Brabletz T, Jung A, Spaderna S, Hlubek F, Kirchner T. Opinion: migrating cancer stem cells - an integrated concept of malignant tumour progression. Nat Rev Cancer. 2005; 5:744–749. [PubMed: 16148886]

Brown KA, Aakre ME, Gorska AE, Price JO, Eltom SE, Pietenpol JA, Moses HL. Induction by transforming growth factor-beta1 of epithelial to mesenchymal transition is a rare event in vitro. Breast Cancer Res. 2004; 6:R215–231. [PubMed: 15084245]

Casas E, Kim J, Bendesky A, Ohno-Machado L, Wolfe CJ, Yang J. Snail2 is an essential mediator of Twist1-induced epithelial mesenchymal transition and metastasis. Cancer Res. 2011; 71:245–254. [PubMed: 21199805]

Dissanayake SK, Wade M, Johnson CE, O'Connell MP, Leotlela PD, French AD, Shah KV, Hewitt KJ, Rosenthal DT, Indig FE, et al. The Wnt5A/protein kinase C pathway mediates motility in melanoma cells via the inhibition of metastasis suppressors and initiation of an epithelial to mesenchymal transition. J Biol Chem. 2007; 282:17259–17271. [PubMed: 17426020]

Dontu G, Abdallah WM, Foley JM, Jackson KW, Clarke MF, Kawamura MJ, Wicha MS. In vitro propagation and transcriptional profiling of human mammary stem/progenitor cells. Genes Dev. 2003; 17:1253–1270. [PubMed: 12756227]

Eirew P, Stingl J, Raouf A, Turashvili G, Aparicio S, Emerman JT, Eaves CJ. A method for quantifying normal human mammary epithelial stem cells with in vivo regenerative ability. Nat Med. 2008; 14:1384–1389. [PubMed: 19029987]

Elenbaas B, Spirio L, Koerner F, Fleming MD, Zimonjic DB, Donaher JL, Popescu NC, Hahn WC, Weinberg RA. Human breast cancer cells generated by oncogenic transformation of primary mammary epithelial cells. Genes Dev. 2001; 15:50–65. [PubMed: 11156605]

Fillmore CM, Kuperwasser C. Human breast cancer cell lines contain stem-like cells that self-renew, give rise to phenotypically diverse progeny and survive chemotherapy. Breast Cancer Res. 2008; 10:R25. [PubMed: 18366788]

Kuhnert F, Davis CR, Wang HT, Chu P, Lee M, Yuan J, Nusse R, Kuo CJ. Essential requirement for Wnt signaling in proliferation of adult small intestine and colon revealed by adenoviral expression of Dickkopf-1. Proc Natl Acad Sci U S A. 2004; 101:266–271. [PubMed: 14695885]

Mani SA, Guo W, Liao MJ, Eaton EN, Ayyanan A, Zhou AY, Brooks M, Reinhard F, Zhang CC, Shipitsin M, et al. The epithelial-mesenchymal transition generates cells with properties of stem cells. Cell. 2008; 133:704–715. [PubMed: 18485877]

Morel AP, Lievre M, Thomas C, Hinkal G, Ansieau S, Puisieux A. Generation of breast cancer stem cells through epithelial-mesenchymal transition. PLoS ONE. 2008; 3:e2888. [PubMed: 18682804]

Oft M, Peli J, Rudaz C, Schwarz H, Beug H, Reichmann E. TΓΦ–β 1 and Ha-Ras collaborate in modulating the phenotypic plasticity and invasiveness of epithelial tumor cells. Genes & Development. 1996; 10:2462–2477. [PubMed: 8843198]

Ogawa K, Saito A, Matsui H, Suzuki H, Ohtsuka S, Shimosato D, Morishita Y, Watabe T, Niwa H, Miyazono K. Activin-Nodal signaling is involved in propagation ofmouse embryonic stem cells. J Cell Sci. 2007; 120:55–65. [PubMed: 17182901]

Onder TT, Gupta PB, Mani SA, Yang J, Lander ES, Weinberg RA. Loss of E-cadherin promotes metastasis via multiple downstream transcriptional pathways. Cancer Res. 2008; 68:3645–3654. [PubMed: 18483246]

Pukrop T, Klemm F, Hagemann T, Gradl D, Schulz M, Siemes S, Trumper L, Binder C. Wnt 5a signaling is critical for macrophage-induced invasion of breast cancer cell lines. Proc Natl Acad Sci U S A. 2006; 103:5454–5459. [PubMed: 16569699]

Rider DA, Dombrowski C, Sawyer AA, Ng GH, Leong D, Hutmacher DW, Nurcombe V, Cool SM. Autocrine fibroblast growth factor 2 increases the multipotentiality of human adipose-derived mesenchymal stem cells. Stem Cells. 2008; 26:1598–1608. [PubMed: 18356575]

Singh A, Settleman J. EMT, cancer stem cells and drug resistance: an emerging axis of evil in the war on cancer. Oncogene. 2010; 29:4741–4751. [PubMed: 20531305]

Suzuki H, Watkins DN, Jair KW, Schuebel KE, Markowitz SD, Chen WD, Pretlow TP, Yang B, Akiyama Y, Van Engeland M, et al. Epigenetic inactivation of SFRP genes allows constitutive WNT signaling in colorectal cancer. Nat Genet. 2004; 36:417–422. [PubMed: 15034581]

Taube JH, Herschkowitz JI, Komurov K, Zhou AY, Gupta S, Yang J, Hartwell K, Onder TT, Gupta PB, Evans KW, et al. Core epithelial-to-mesenchymal transition interactome gene-expression signature is associated with claudin-low and metaplastic breast cancer subtypes. Proc Natl Acad Sci U S A. 2010; 107:15449–15454. [PubMed: 20713713]

Thiery JP, Acloque H, Huang RY, Nieto MA. Epithelial-mesenchymal transitions in development and disease. Cell. 2009; 139:871–890. [PubMed: 19945376]

Toda H, Tsuji M, Nakano I, Kobuke K, Hayashi T, Kasahara H, Takahashi J, Mizoguchi A, Houtani T, Sugimoto T, et al. Stem cell-derived neural stem/progenitor cell supporting factor is an autocrine/paracrine survival factor for adult neural stem/progenitor cells. J Biol Chem. 2003; 278:35491–35500. [PubMed: 12832409]

Veeman MT, Slusarski DC, Kaykas A, Louie SH, Moon RT. Zebrafish prickle, a modulator of noncanonical Wnt/Fz signaling, regulates gastrulation movements. Curr Biol. 2003; 13:680–685. [PubMed: 12699626]

Yang J, Mani SA, Donaher JL, Ramaswamy S, Itzykson RA, Come C, Savagner P, Gitelman I, Richardson A, Weinberg RA. Twist, a master regulator of morphogenesis, plays an essential role in tumor metastasis. Cell. 2004; 117:927–939. [PubMed: 15210113]

Zeisberg M, Hanai J, Sugimoto H, Mammoto T, Charytan D, Strutz F, Kalluri R. BMP-7 counteracts TΓΦ–β1-induced epithelial-to-mesenchymal transition and reverses chronic renal injury. Nat Med. 2003; 9:964–968. [PubMed: 12808448]

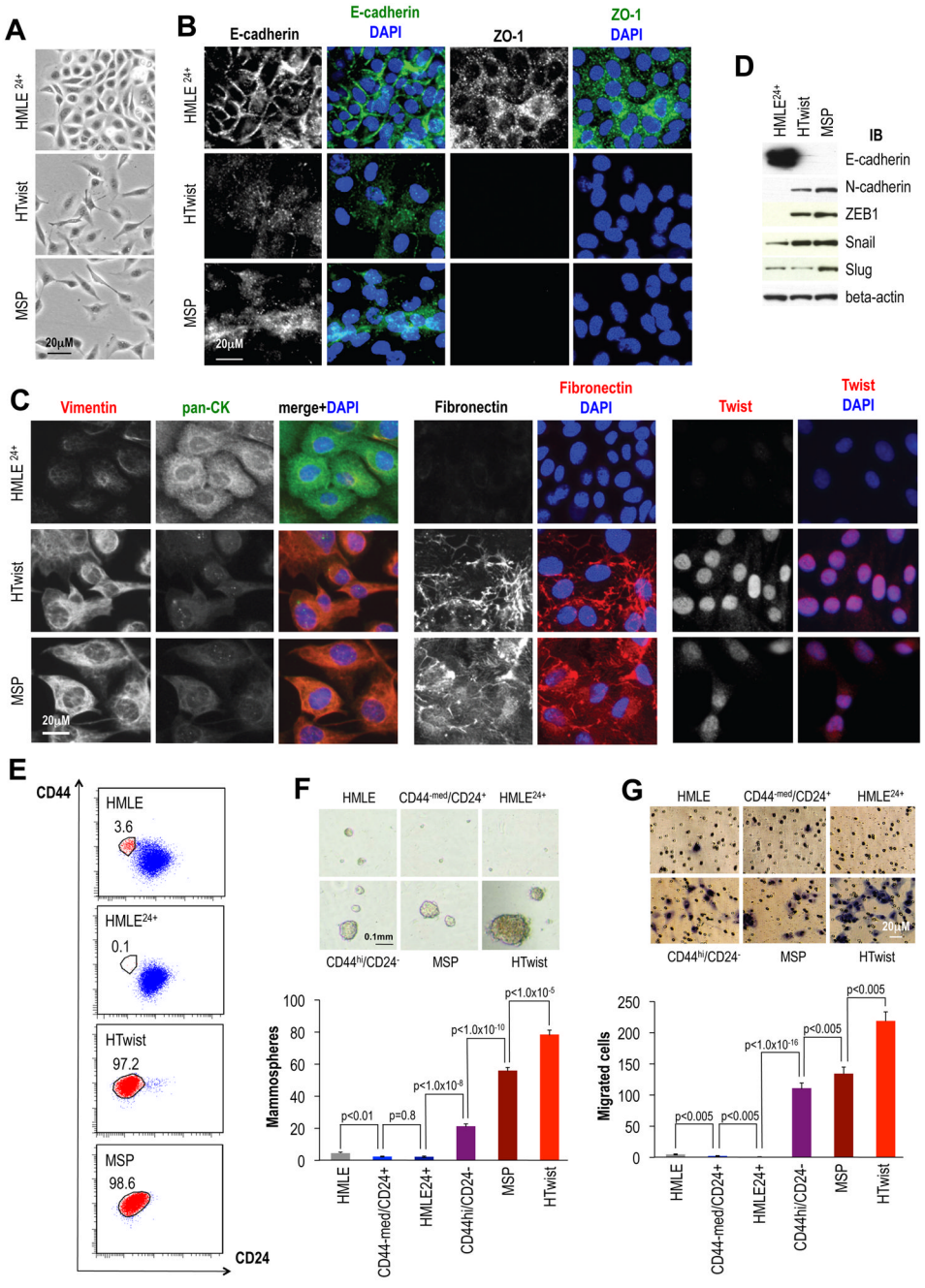

Figure 1. A mesenchymal subpopulation (MSP) isolated from immortalized human mammary epithelial cells (HMLE) cells

(A) Bright phase microscopy: MACS-purified HMLE^{24+}, HMLE overexpressing Twist (HTwist) and re-attached MSP cells. (B) Immunofluorescence: adherens junction protein E-cadherin and tight junction protein ZO-1 in HMLE^{24+}, HTwist and MSP cells. (C) Immunofluorescence: mesenchymal intermediary filament vimentin and epithelial cytokeratins (panCK = pan-cytokeratin antibody), expression of fibronectin and Twist. (D) Immunoblot: E- and N-cadherin, EMT-TFs ZEB1, Snail and Slug, loading control: β-actin. (E) Flow cytometry: CD44-APC and CD24-PE cell-surface staining. Numbers indicate % of CD44^{hi}/CD24^{-} population. (F) Mammosphere Assay: bright phase microscopy images and

quantification of parental HMLE, HMLE^{24+}, HTwist and MSP as well as FACS-purified CD44^{hi}/CD24^{-} and CD44$^{-med(ium)}$/CD24^{+} HMLE cells; n=12. (G) Migration assay: microscopy images and quantification; n=3.

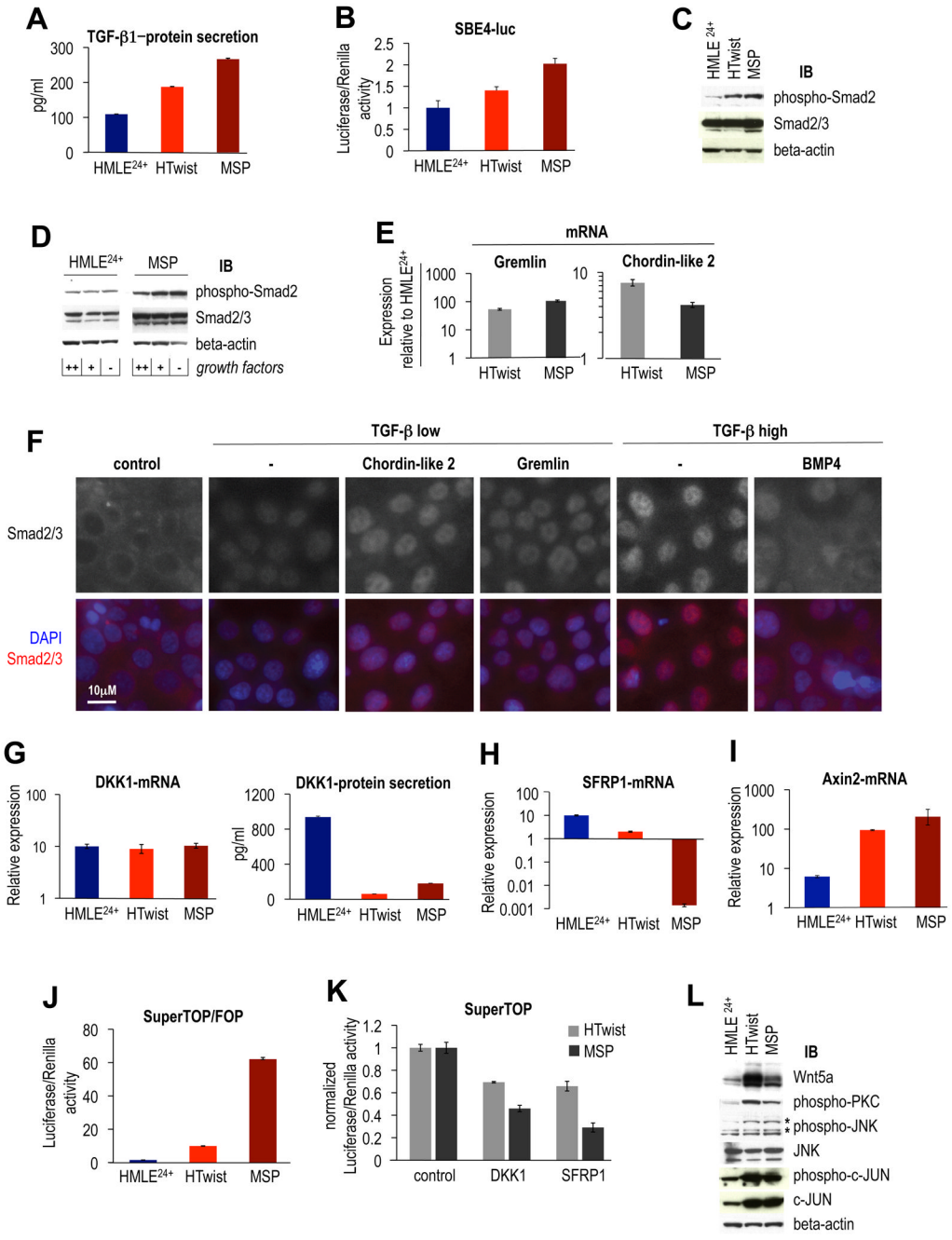

Figure 2. EMT-associated autocrine signaling

(A) ELISA: TGF–β1 secretion by HMLE^{24+}, HTwist and MSP cells, n=3. (B) Luciferase reporter assay: Smad transcriptional activity: cells were transfected with SBE4-luc reporter plasmid, firefly luciferase levels were normalized to pGL-SV40 renilla transfection control, n=3. (C) Immunoblot: Smad2 phosphorylation in HMLE^{24+}, HTwist and MSP cells. Loading control: β-actin. (D) Immunoblot: Smad2 phosphorylation, loading control: β-actin. Cells were cultivated 24h in full medium (++), growth factors reduced by 90% (+), or growth factor-free (−). (E) RT-PCR: mRNA expression of BMP antagonists Gremlin, Chordin-like 2, both relative to HMLE^{24+} cells. (F) Immunofluorescence: modulation of Smad2/3 nuclear translocation by BMP-antagonists and –ligand. HMLE^{24+} cells were

stimluated with TGF–β1 (low: 0.3ng/ml, high: 2.5ng/ml) alone or together with Chordin-like 2, Gremlin (both 2.5μg/ml) or BMP4 (0.5μg/ml) for 30min. (G) RT-PCR: DKK1-mRNA expression, ELISA: DKK1-protein secretion, n=3. (H) RT-PCR: SFRP1-mRNA expression. (I) RT-PCR: Axin2-mRNA expression. (J) Luciferase reporter assay (TOPFlash): cells were transfected with Super(8x)TOP (TCF-LEF reporter) or FOP construct (mutated binding sites). Shown is TOP over FOP firefly luciferase activity, normalized to pGL-SV40 renilla transfection control, n=3. (K) Inhibition of TOPFlash activity: DKK1 or SFRP1 protein (1.0 μg/ml) were added to the growth medium of HTwist and MSP for 12h, n=3. (L) Immunoblot: PKC and JNK pathways associated with non-canonical Wnt signaling. Phospho-JNK antibody generated an unspecific bottom band, asterisks point to phosphorylated SAPK/JNK isoforms. Loading control: β-actin

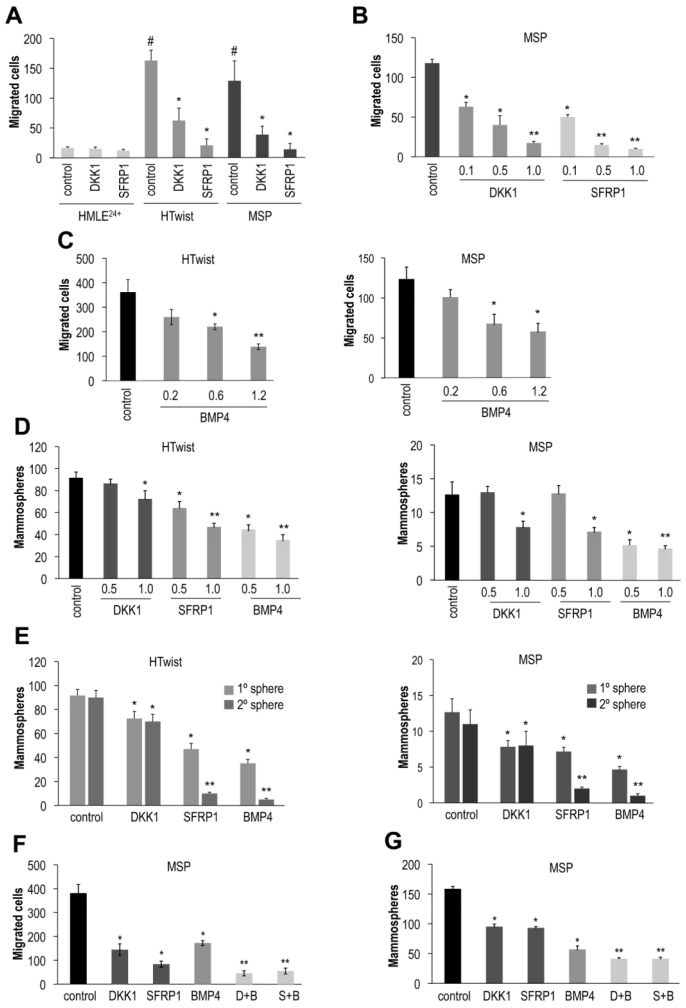

Figure 3. Autocrine Signaling controls migration and mammosphere formation

(A) Migration assay: DKK1 or SFRP1 protein (0.5μg/ml) was added to growth medium; #HMLE control vs. HTwist and MSP control, $p<1\times10^{-6}$, *HTwist or MSP control vs. treatment with DKK1 or SFRP1, $p<1\times10^{-6}$, n=3. (B) Migration assay: dose-dependent inhibition of migration by DKK1 or SFRP1 protein at indicated concentrations (μg/ml), n=3; *H-Twist or MSP control vs. treatment with DKK1 or SFRP1, $p<1\times10^{-6}$, ** H-Twist or MSP, high vs. low concentration, $p<1\times10^{-7}$, n=3. (C) Migration assay: dose-dependent inhibition of migration by recombinant BMP4 protein at indicated concentrations (μg/ml); *HTwist or MSP control, $p<0.05$, **0.6μg/ml vs. 1.2 μg/ml, $p<1\times10^{-4}$, n=3. (D) Mammosphere formation: DKK1, SFRP1 or BMP4 protein were added daily during sphere formation (5d) at indicated concentrations (μg/ml); *HTwist or MSP control vs. treatment, $p<0.01$, **low vs. high concentration or recombinant protein, $p<0.05$, n=8. (E) Secondary mammosphere formation: DKK1 (1μg/ml), SFRP1 (1μg/ml) and BMP4 (0.5μg/ml) were added daily during primary sphere formation (5d), primary spheres were dispersed and seeded for secondary sphere formation in the absence of further treatment; *H-Twist or MSP control vs. treatment, $p<0.01$, **primary vs. secondary sphere number, $p<0.01$, n=16. (F) Mammosphere assay: HTwist cells were treated daily during mammosphere formation (5d) with proteins as described in (B), D+B: DKK1 and BMP4 were added together, S+B: SFRP1 and BMP4 were added together; *control vs. single treatment, $p<1\times10^{-5}$, **single vs. double-treatment, $p<0.01$, n=6. (G) Migration Assay: HTwist cells were seeded into

Boyden Chambers in the presence of DKK1 (1μg/ml), SFRP1 (1μg/ml), BMP4 protein (0.5μg/ml) or in combination as indicated in (F); *control vs. single treatment, $p<1\times10^{-5}$, **single vs. double-treatment, $p<0.01$, n=3.

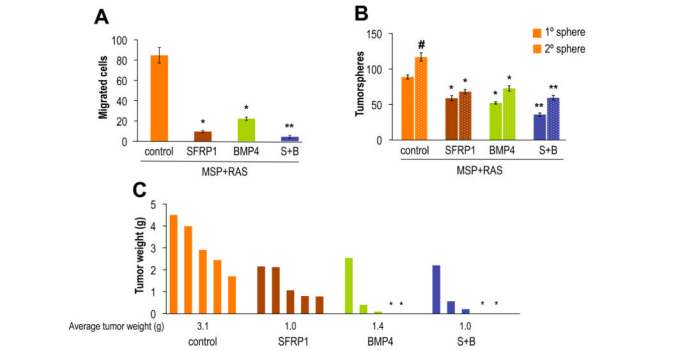

H

Number of cells injected:	Tumor incidence/ Number of injections			
	control	SFRP1	BMP4	S+B
$5x10^5$	5/5	5/5	3/5	3/5
$5x10^4$	10/10	4/10	4/10	4/10
$5x10^3$	4/5	1/5	1/5	0/5

Figure 4. Autocrine Signaling controls tumorigenicity and metastasis

(A) Migration assay: SFRP1 (1μg/ml) and BMP4 protein (0.5μg/ml) were added to growth medium; *control vs. single treatment, $p<1\times10^{-8}$, **single vs. double treatment with SFRP1 and BMP4 (S+B), $p<1\times10^{-4}$, n=3. (B) Tumorsphere assay: SFRP1 (1μg/ml) and BMP4 protein (0.5μg/ml) were added daily during primary sphere formation (5d), spheres were dissociated and seeded for secondary sphere formation in the absence of further treatment; #control primary vs. secondary sphere formation, p=0.001; *control vs. single treatment, $p<1\times10^{-4}$, **single vs. double treatment with SFRP1 and BMP4 (S+B), p<0.01, n=6. (C) Orthotopic tumor formation after *ex vivo* treatment: primary tumorspheres as generated in (B) were pooled, dissociated and 1.0×10^5 cells were implanted in the mammary fat pads of mice; shown is tumor weight, *indicates absence of tumor, n=5 mice/group. (D) Lung metastasis: fluorescence microscopy images with magnified insets of the major left lung lobe showing GFP-positive metastatic foci. (E) Quantification of lung surface metastatic foci; *control vs. SFRP1 treatment, p<0.05, **SFRP1 vs. BMP4 or double treatment (S+B), p<0.05, n=5 mice/group. (F) Liver metastasis: fluorescence microscopy images and magnified insets of the liver surface showing GFP-positive micro-metastatic foci after implantation of cells as described in (D). (G) Quantification of liver surface metastastatic foci: 5 fields of liver surface were counted per mouse, *control vs. single treatment, p<0.05, **single vs. double treatment (S+B), p<0.05, n=5 mice/group. (H) Tumorigenicity assay: MSP-RAS cells suspended in PBS containing SFRP1 (1μg/ml), BMP4 (0.5μg/ml), and a combination of both (S+B) were implanted subcutaneously in mice at indicated cell numbers. In addition, 20μl of PBS or PBS containing recombinant protein was injected peri-tumorally at 1, 2, 3 and 7d post implantation.

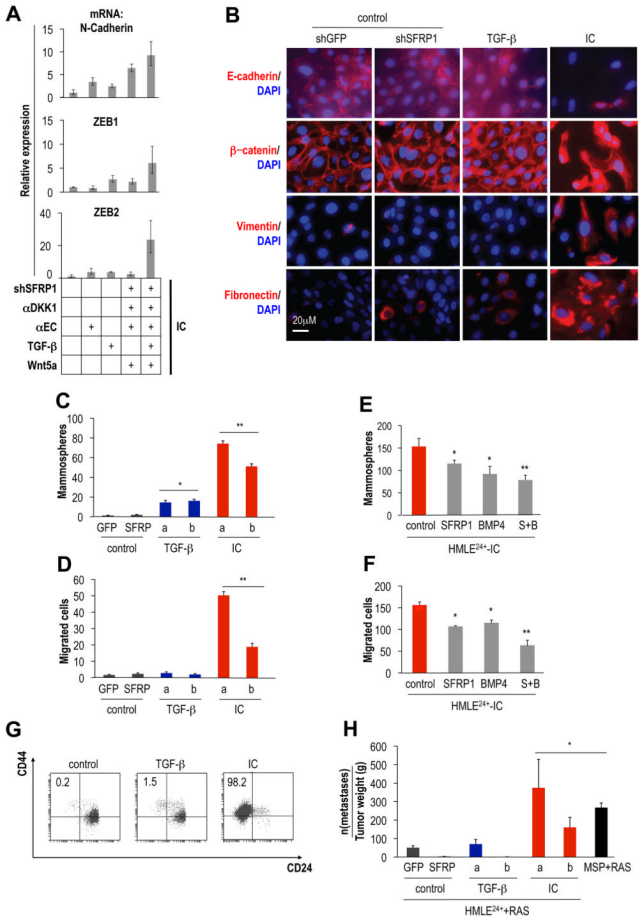

Figure 5. Creation of a permissive extracellular environment for EMT-induction

(A) RT-PCR: mRNA expression of N-cadherin, ZEB1 and ZEB2, all relative to untreated control cells (HMLE^{24+}-shGFP). HMLE^{24+}-shGFP or -shSFRP1 (shRNA-mediated knockdown of SFRP1, Figure S5B) were treated for 3d daily: anti-DKK1 antibody (αDKK1, 100μg/ml), antiE-cadherin antibody (αEC, 10μg/ml), TGF–β1 (2.5ng/ml), Wnt5a (250ng/ml). All factors added together to HMLE^{24+}-shSFRP1 constitutes the induction cocktail (IC). (B) Immunofluorescence: E-cadherin, beta-catenin, vimentin and fibronectin expression in control (HMLE^{24+}-shGFP and HMLE^{24+}-shSFRP1), TGF–β-treated HMLE^{24+}-shGFP and IC-treated HMLE^{24+}-shSFRP1 cells (14d of treatment). (C) Mammosphere (n=7) and (D) Migration assays (n=3): cells generated as indicated in (B): a and b indicate independently treated replicates, *control vs. TGF–β treatment, $p<1\times10^{-4}$, **control vs. IC treatment, $p<1\times10^{-9}$. (E) Mammosphere (n=6) and (F) Migration assay (n=3): cells were expanded for 12 passages after cessation of treatment as described in (B), then seeded into assays in presence of SFRP1 (1μg/ml/d), BMP4 (0.5μg/ml/d) or both (S+B) proteins, *control vs. single treatment, $p<0.01$, **single vs. double treatment (S+B), $p<0.05$. (G) Flow cytometry: CD44-APC and CD24-PE cell-surface staining in control, TGF–β and IC-treated cells generated as described in (B). Numbers indicate percentage of CD44^{hi}/CD24^{-} population. (H) Lung metastasis: cells expanded for 8 passages after cessation of treatment as described in (B) were transformed with RAS; cells were injected into the mammary fat pads of mice; GFP-labeled metastases on the surface of the lungs were quantified; *control vs. all other groups, $p < 0.05$, n=5 mice/group.

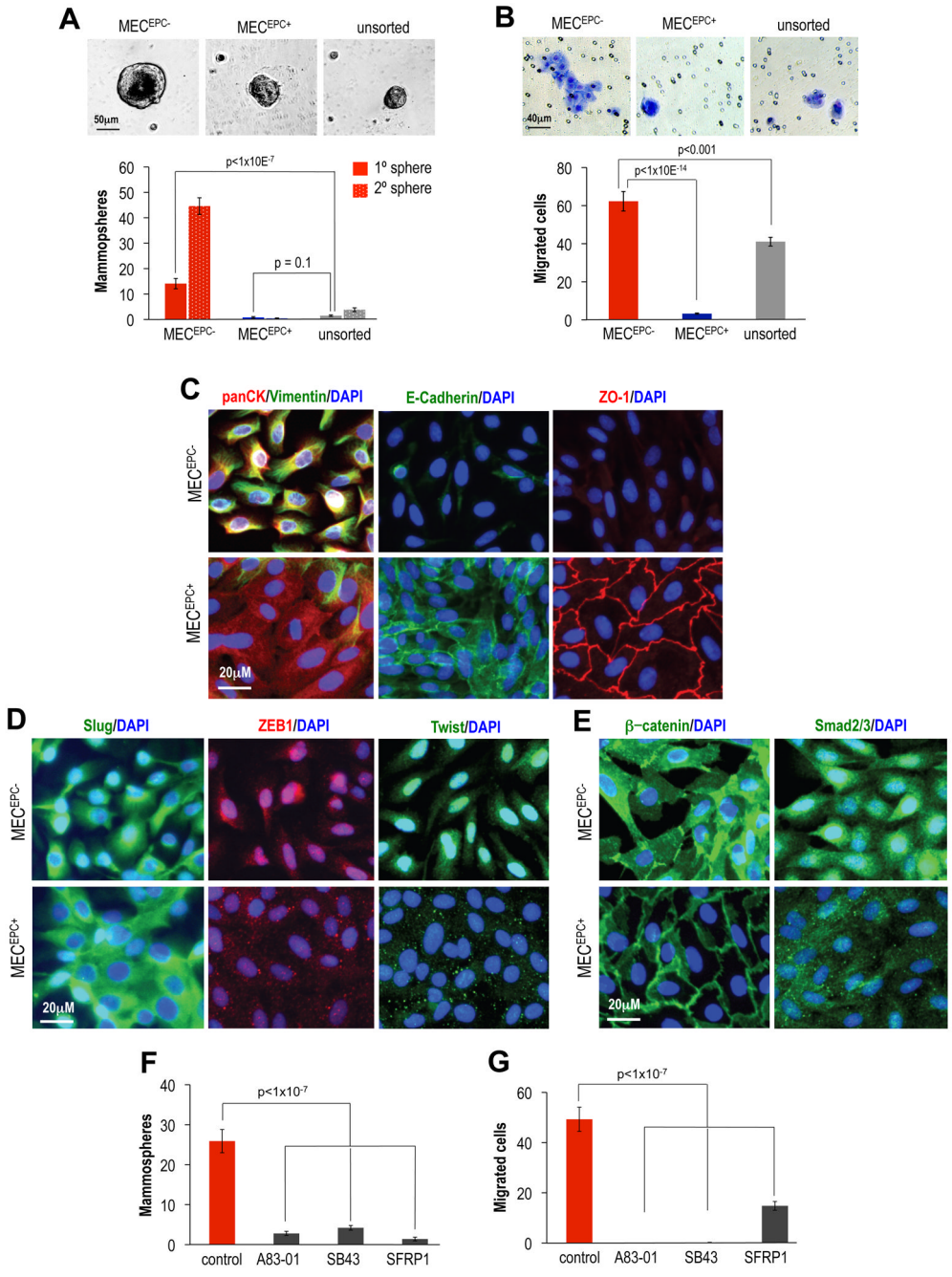

Figure 6. Characterization of primary mammary epithelial cell (MEC) populations enriched in self-renewal and motility

(A) Mammosphere Assay: microscopy images of mammospheres and quantification of mammosphere formation by FACS purified MEC^{EPC-}, MEC^{EPC+}, unsorted MEC (Figure S6A), after 5d of monolayer culture. Primary spheres formed over a period of 7d were dissociated and seeded for secondary sphere formation, n=48. (B) Migration Assay: microscopy images of migrated cells and quantification, n=6 wells. (C) Immunofluorescence: expression of mesenchymal and epithelial markers in MEC^{EPC-}, MEC^{EPC+} after 5d of monolayer culture; vimentin, pan-cytokeratin (panCK), E-cadherin, ZO-1 and (D) EMT-TF Twist, Slug and ZEB1 and (E) beta-catenin and Smad2. (F)

Mammosphere Assay: MEC^{EPC-} were seeded into assay after a 5d pre-treatment with TGFBRI-inhibitors A83-01, SB435142 (SB43, both at 10μM) and recombinant SFRP1 (1μg/ml), n=24. (G) Migration Assay: MEC^{EPC-} were seeded into migration assays after 5d pre-treatment as described in (C), n=6.

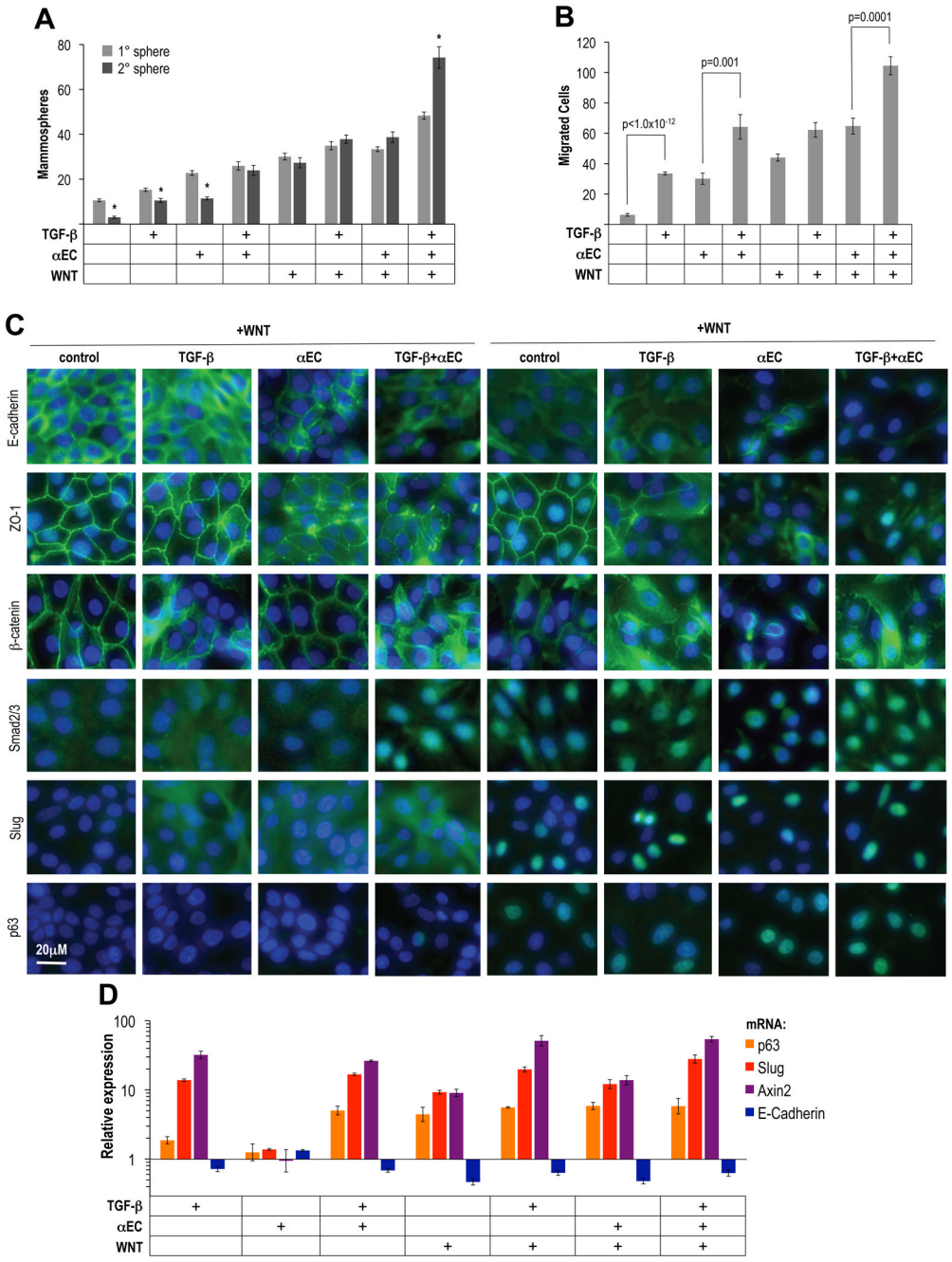

Figure 7. Wnt and TGF–β signals govern conversions between basal and luminal MEC

(A) Mammosphere assay: FACS purified MEC^{EPC+} were cultured for 3d in the presence of Wnt-pathway stimulating factors referred to as WNT (anti-DKK1 antibody (100μg/ml), anti-SFRP1 antibody (2μg/ml), recombinant Wnt5a (250ng/ml), followed by 2d in the additional presence of recombinant TGF–β1 (0.1ng/ml), anti-E-cadherin antibody (αEC, 20μg/ml) or a combination of both. Secondary spheres were generated by dissociation of primary spheres. *Primary vs. secondary sphere forming cells, $p<0.0005$, n=10. (B) Migration assay: before plating into Boyden Chambers MEC^{EPC+} were treated as described in (A), n=3. (C) Immunofluorescence: MEC^{EPC+} were treated as described in (A) and expanded for 2d in the absence of further treatment: expression of E-cadherin, ZO-1, beta-catenin, Smad2, Slug and

p63. (D) RT-PCR: mRNA expression of p63, Slug, Axin2 and E-cadherin in MEC^{EPC+} after treatment as described in (A), followed by expansion for 2d in the absence of further treatment.